論文 / 著書情報
Article / Book Information

Title	Suffusion-induced change in spatial distribution of fine fractions in embankment subjected to seepage flow
Authors	Kazuki Horikoshi, Akihiro Takahashi
Citation	Soils and Foundations, Vol. 55, Issue 5, pp. 1293-1304
Pub. date	2015, 10
DOI	http://dx.doi.org/10.1016/j.sandf.2015.09.027
Creative Commons	See next page.
Note	This file is author (final) version.

License

Title:

Suffusion-induced change in spatial distribution of fine fractions in embankment subjected to seepage flow

Author 1:

Kazuki Horikoshi

Graduate student, Department of Civil Engineering, Tokyo Institute of Technology, Tokyo, Japan

Author 2, Corresponding author:

Akihiro Takahashi

Professor, Department of Civil Engineering, Tokyo Institute of Technology, Tokyo, Japan

Full contact details of corresponding author.

Akihiro Takahashi (Author 2)

2-12-1-M1-3 Oh-okayama, Meguro, Tokyo 152-8552

Tel: 03-5734-2593, E-mail: takihiro@cv.titech.ac.jp

Soils and Foundations, 55(5), 1293-1304, 2015

Original URL:

http://dx.doi.org/10.1016/j.sandf.2015.09.027

Abstract

Suffusion describes the phenomenon whereby finer particles are eroded through the voids of coarse particles by the seepage flow. This may cause the deterioration of the hydraulic structure and, in the worst case, result in the failure of the hydraulic structure. The suffusion process is presented in this paper in an embankment under transient and steady seepage conditions. A series of physical model tests on seepage-induced suffusion on a small-scale model embankment is performed under constant boundary head conditions. A binary mixture, consisting of two Silica sands (Silica sands Nos. 3 and 8), which is categorized as “internally unstable material” by several previous criteria for the seepage-induced internal stability, is used for the model embankment. The cumulative eroded soil mass and the discharged rate of water are recorded during the seepage tests. The spatial extent of the variation in erosion-induced fines contents is discussed through sieve analyzes on subdivided areas of the model embankment after seepage testing. The test results reveal that a decrease in fines propagates along the phreatic surface from downstream in the embankment. Below the phreatic surface, the eroded fines not only move laterally by the seepage flow, but also vertically due to the gravitational force, and are deposited in the foundation. This deposition of the fines results in the expansion of the fine-rich region in the foundation and causes a decrease in the permeability of the whole embankment.

Keyword: suffusion; internal erosion; seepage; physical model tests

International Geotechnical Classification System

E07

1. Introduction

Erosion induced by seepage inside embankments is called internal erosion. This phenomenon is known to be one of the causes of the deterioration of hydraulic structures and, in severe cases, triggers the failure of the structures (e.g., Foster et al., 2000; Richards and Reddy, 2007; Fry et al., 2012). Ground disasters caused by this phenomenon have not only occurred in hydraulic structures, but also in reclaimed land (Khomenko, 2006; Kuwano et al., 2012).

Types of internal erosion include concentrated leak erosion, contact erosion, backward erosion, and suffusion (Fry, 2012; Fell and Fry, 2013). Concentrated leak erosion is driven by the seepage flow in the opening (crack or cavity). It detaches particles from the sides of the opening. Contact erosion is the erosion of particles at the interface between fine and coarse layers due to a quasi- horizontal groundwater flow. Backward erosion describes the erosion of soil particles at the exit end of a seepage path, such as leaking through the downstream surface due to a high exit velocity or hydraulic gradient. Suffusion describes the phenomenon whereby finer particles are eroded through the voids between the coarse particles by the seepage flow. It is also described as “a special case of backward erosion peculiar to gap-graded soil” (Richards and Reddy, 2014). This paper focuses on the suffusion phenomenon.

The process of dam failure by internal erosion and piping is classified into four phases: the initiation of erosion, the continuation of erosion, the progression to form a pipe, and the formation of a breach (Foster and Fell, 1999). Foster and Fell (1999) described this erosion process by detailed event trees. Some of the steps of this process show how failure initiated due to suffusion in an embankment or its foundation; this is the target of the present study.

Moffat et al. (2011) defined suffusion as the phenomenon whereby “the finer fraction of an internally unstable soil moves within the coarser fraction without any loss of matrix integrity or change in total volume,” whereas with suffosion, “particle migration yields a reduction in total volume and a consequent potential for collapse of the soil matrix”. In this paper, the widely accepted term “suffusion” is used.

Suffusion develops in the first two phases, namely, the initiation of erosion and the continuation of erosion, in the failure scenarios initiated by suffusion. This phenomenon is a potential risk to the long-term stability of hydraulic structures over a period of years. During these phases, the performance of a hydraulic structure, e.g., the hydraulic and mechanical characteristics, might deteriorate progressively. On the other hand, the time scale for the third and fourth phases related to piping, namely, the progression to form a pipe and the formation of a breach, are relatively short, compared with the time scale for the first two phases. In other words, the hydraulic structure is in the phases of the initiation or the continuation of erosion for most of its service life. Therefore, this study focuses on the suffusion development phase and includes the initiation of erosion and the continuation of erosion phases.

For the initiation of erosion phase in the failure process of embankment dams, many research works have been conducted on suffusion and internal instability based on one-directional upwards or downwards seepage experiments; the initiation of this phenom- enon depends on the particle size ratio between the finer fraction and the coarse fraction (e.g., Honjo et al., 1996; Terzaghi, 1939), the particle size distribution (e.g., Kenney and Lau, 1985; Li and Fannin, 2008; Wan and Fell, 2008; Chang and Zhang, 2013; Moraci et al., 2014), the particle shape (Marot et al., 2012), the confining pressure (e.g., Bendahmane et al., 2008; Moffat and Fannin, 2011), the hydraulic gradient (e.g., Skempton and Brogan; 1994, Sterpi, 2003), the flow velocity (Perzlmaier et al., 2007), and the seepage angle (Richards and Reddy, 2012, 2014), among other factors. Richards and Reddy (2014) suggested a methodology based on kinetic energy to predict suffusion and the backward erosion initiation potential and performed analyses of the factors of safety against these phenomena for a homogenous embankment model with a foundation.

For the continuation of erosion phase, the development of erosion depends on the presence or absence of an adequate filter or transition zone (Foster and Fell, 1999). Moffat et al. (2011) showed the spatial and temporal progression of seepage-induced internal instability, which included suffusion and suffosion from the initiation to the progression phases in a one-dimensional seepage field. They observed the conditions of the specimen through a transparent wall and measured the local hydraulic gradient in the specimen. Luo et al. (2012) described the evolution of suffusion in pore scale as: "fine particles migration-pores clogging-pushing out clogging pores-fine particles remigration." These observations were made in the laboratory in a relatively short period, i.e., days. However, the time scale for the initiation and the continuation of suffusion phases in a real embankment or foundation is very slow, i.e., from months to years (Fell et al., 2003).

Most of the above-mentioned suffusion studies focused on the phenomenon in a uniform one-dimensional seepage field, while the seepage flow in a real structure is more complex and so is the suffusion progress. However, there are few studies which consider the effect of the geometry of a real structure on suffusion in the initiation and the continuation phases. The laboratory experiments of Lindow et al. (2009) suggested that the failure mechanism due to seepage is dependent on the slope angle. Sterpi (2003), Cividini and Gioda (2004) and Cividini et al. (2009) carried out finite element analyses to examine the spatial and temporal distributions of fines under seepage with a phreatic surface by modifying the erosion model proposed by Sterpi (2003). Uzuoka et al. (2012) and Zhang et al. (2013, 2014) demonstrated the temporal change in fines within the "geometry" of the embankment by means of numerical simulations.

Experimental studies on internal erosion have been con- ducted for large-scale contact erosion (Beguin et al., 2012). To the authors' knowledge, studies based on physical model tests for suffusion are limited (Saito et al., 2012). Saito et al. (2012) provided eight hours of water supply, 16 h of drainage and 180 repetitions to a physical model, which was made of pit sand to imitate a levee. After seepage testing, the fines content was examined at four locations within the model levee.

In this paper, a series of physical model tests is performed on a small-scale model to examine the seepage-induced suffusion process in an embankment during the phases of the initiation and the continuation of erosion.

2. Experimental apparatus and procedure

2.1 *Material*

To simplify the phenomenon, a mixture of fine and course fractions, namely, a gap-graded soil, is used for the model. This type of gap-graded soil exists in the glacial tills of Canada and New Zealand, but sometimes is used as material for filling. To use a dredged soil as a fill material, its workability is improved by mixing in cement or pit sand. Typically, the latter is a gap-graded soil. Although use of such a material can exaggerate the test results, it allows (a) easy distinction between the base and the erodible materials and (b) easy observation of the fines migration in a short period.

Based on the works by Ke and Takahashi (2012, 2014), Silica sands Nos. 3 and 8 are used as the model materials. Silica sand No. 3 is applied to model the soil skeleton, while Silica sand No. 8 is applied as the erodible fines particles in the voids of the coarse skeleton. Hereafter, Silica sand No. 8 is referred to as fines for simplicity, even though Silica sand No. 8 is not strictly classified as fines by the Japanese Industrial Standards (JIS). The chosen fines content of the mixture is 15%. The particle size distribution curves for each type of sand are shown in Fig. 1, while the mixture and the basic properties of the mixture material are shown in Table 1.

According to several criteria on seepage-induced internal stability (Chang and Zhang, 2013; Wan and Fell, 2008; Li and Fannin, 2008), the mixture used in this study is categorized as “Internally unstable material” and it is vulnerable to suffusion if seepage takes place. The calculated critical hydraulic gradient for zero effective stress is 1.0 according to Terzaghi's equation. Ke and Takahashi (2012) performed a series of one- dimensional upward seepage tests on a similar mixture with fines contents of 14.3, 16.7, 20, and 25%. Their critical gradient for suffusion, i_{sc}, was linearly correlated with the fines content, FC ($i_{sc} = -0.0037FC + 0.302$, $R^2 = 0.997$). From this linear relationship, the expected critical gradient against suffusion for the mixture used in this study (15% fines content) is 0.25.

Permeability tests are conducted on specimens with varying fines contents (FC = 2.5–30.0%) under a constant void ratio of the coarse skeleton (void ratio of the coarse skeleton, e_s = 0.885; relative density of the coarse skeleton, Dr_s = 40%) in accordance with JIS and Japanese Geotechnical Society (JGS) standards. In the tests, a small hydraulic gradient is imposed so that suffusion does not occur during the tests. Fig. 2 shows the relationship between hydraulic conductivity and the fines contents. In physical model tests, described later, the model embankment is made of partially saturated soil containing tap water. For these reasons, permeability tests are conducted on (a) soil that has been partially saturated with tap water and (b) soil that has been fully saturated with deaired water. Fig. 2 indicates that the hydraulic conductivity of a specimen without deairing is lower than that of a fully saturated one. It should also be noted that, even at the same fines content, the packing of the fines may not be the same for these two conditions because the position of the fines in the voids of the coarse skeleton are different depending on whether or not air bubbles exist in the voids.

2.2 *Experimental apparatus*

The embankment models are made in a steel box with inner dimensions of 500 mm × 150 mm × 350 mm, as shown in Fig. 3(a). The box has two tanks on both sides, namely the "water supply tank" and the "drainage tank." The vertical sidewalls between the tank and the embankment model contain a metal mesh so that only water and fines less than 0.25 mm can flow through them. By pouring water into the water supply tank, the seepage flow in the ground can be modeled. The boundary heads reach 190 mm and 40 mm at the upstream and downstream sides, respectively, in around 30–40 min for all cases. Seepage water from the model embankment eventually passes through the drainage tank and finally discharges from the outlet. The drainage tank has two holes, one is to discharge the eroded soil and some quantity of water (a small hole located at a level of 0 mm) and the other is to maintain a constant head (a large hole located at a level of 40 mm).

As shown in Fig. 3(b), the discharged soil and water flow into a small container via an aluminum angle. The small container is filled with water to a constant level and is located near the steel box. Eroded fines are collected in a bowl that is suspended on wires under the water inside the small container. To prevent the outflow of fines to the outside of the bowl and to help the sedimentation of fines, the bowl is covered with filter paper on the side surface. The cumulative eroded mass is recorded automatically by a load cell (Kyowa Electronic Instruments Co., Ltd., LVS-2KA, measureable range: 0–20 N) connected to the wires. The calibration of the load cell is performed before each seepage test, and the mass balance is also checked by the amount of collected eroded soil after each test.

To prevent material separation during the preparation of the model embankment, the moist tamping method (Ladd, 1978) is employed. The soil is compacted in layers, with a thickness of 20 mm, where no sensors are located. The pore pressure transducers used here are SSK Micro Pressure Transducers P306V-01 (measurable range: 0–10 kPa). To avoid the formation of a concentrated water path along the wiring of the sensors, the pore pressure transducers are placed near the back side of the steel box. An effort is made to measure the pore water pressure properly. However, the response of the sensor output was not so sharp, i.e., full saturation of the sensors may not have been achieved, since the tests started from the state in which the model embankment was under partially saturated conditions with a small water content. Even so, the sensor readings can be used to detect the arrival of water and to measure the changes in pore water pressure. The target dry density is 1.560 g/cm^3 (void ratio, e = 0.695; relative density, Dr = 35%). The initial moisture content is 3.0%. After making the level ground, the model ground is scraped off with a shaped frame and formed to be a 260.5-mm-high embankment. To prevent the occurrence of a strong flow between the side wall and the model, a mixture of grease and silicon oil is put on the inside surface of the wall.

The model embankment is composed of two areas, the “foundation zone” and the “slope zone” (includes the “slope zone” and the “lower section of the crown”), as shown in Fig. 3(a). The foundation zone is an 80-mm-thick horizontal layer and the slope zone is an embankment with a slope of 1:1.8. According to a statistical survey of dam failures, this type of zoning, which has no zoning of materials or downstream filter, is most vulnerable to internal erosion (Foster and Fell, 2001; Fry et al., 2012).

As far as the saturated seepage flow is concerned, the hydraulic gradient field in the model embankment is similar to a possible prototype, provided that the geometry of the embankment and the water head at the boundaries are consistent. However, if a phreatic water surface exists and internal erosion is involved, the following problems may arise and create limitations to this experiment: (1) the relative position of the phreatic surface in the small-scale model becomes higher than that in the prototype because the amount of capillary rise does not change with the model scale; and (2) the erosion-induced contractive deformation in the small- scale model can be diminished, since a soil becomes more dilative under small confining pressure. In addition to these problems, the confining pressure dependency of the fines loss is another concern. Ke and Takahashi (2014) carried out a series of one-dimensional downward seepage tests on a similar mixture with a fines content of 35% under several levels of confining pressure and showed that the erosion potential decreases with an increasing confining pressure. Bendahmane et al. (2008) also showed a similar tendency for different internally unstable soil. Moffat et al. (2011), and Moffat and Fannin (2011) demonstrated that an increase in effective confining pressure would cause an increase in the critical hydraulic gradient for erosion. Tomlinson and Vaid (2000) investigated the effect of the confining pressure on the initiation of piping experimentally. Their results indicate that (a) the confining pressure has a certain influence on the internal stability if the ratio between the course and fines particles is not so large and (b) particle size ratio D_{15c}/d_{85f} is the most important parameter for the initiation of piping.

Considering these results, the stress level of an embankment may have little effect on suffusion. Therefore, useful data on the spatial changes in the fines content can be obtained by physical model tests in small-scale models.

2.3 *Experiment procedures and conditions*

In this study, the seepage flow stages of a transient seepage condition (first permeation to partially saturated model) and a steady seepage condition are reproduced using the above experimental system. First, the transport of fines in the above-mentioned stages is examined. By controlling the water level at the upstream boundary, the influence of repeated permeation on the spatial change in the fines in the embankment is also examined. Detailed test conditions and a conceptual diagram of the controlled water level at the upstream boundary are summarized in Table 2 and Fig. 4. The elapsed time is measured by the pouring of water into the water supply tank. The seepage flow in the embankment reaches a nearly steady condition in 30–40 min.

A total of eight tests are conducted. *Case St1* is conducted to investigate the erosion during the first permeation stage (unsteady seepage condition) and the test is terminated as soon as the steady seepage condition is reached (Fig. 4). In the other cases (*Cases St20*, *St24*, *St48*, and *St280*), the seepage is continued for a prescribed time while keeping the water heads at the boundaries constant.

Cases St96RS4, *St96RS8*, and *St280RS40* are carried out to assess the influence of the raising and the lowering of the phreatic surface on the spatial changes in the fines in the embankment. *Case St96RS4* consists of 1440 min of water supply, 1440 min of drainage, and four repetitions to the physical model. In *Case St96RS8*, repeated water penetrations are provided in eight cycles of 720 min. In this case, the value of the pore water pressure transducer at P1 in Fig. 3(a) shows a maximum head fluctuation of plus or minus 50 mm due to complications in the experimental system. In *Case St280RS40*, the repeated permeation times are random. The objective of *Case St280RS40* is to understand how the spatial distribution of the fines in the embankment is affected by the raising and the lowering of the phreatic surface. To exaggerate the spatial change in the fines, the raising and the lowering of the water level at the upstream are randomly conducted as many times as possible.

During the seepage tests, the crown settlement is measured by displacement sensors. However, even in *Cases St280* and *StRS40*, which showed relatively large settlements, the maximum values were 0.16 mm and 0.21 mm at the top of the slope and 0.06 mm and 0.24 mm at the center of the crown during the seepage tests. Compared with the initial model height of 260.5 mm, it can be said that the overall change in volume of the model embankment is negligible. Therefore, the volume change of the embankments is not considered in this study.

After the seepage tests, a sieve analysis is carried out in each area of the embankment to estimate the extent of the variation in erosion-induced fines contents. Soils are sieved in a dry condition. This is because the non-plastic sample, with a large grain size ratio of coarse to fine components, is easily separated. This test is conducted once per each divided element. For each test, the sieves are cleaned with a vibrator, an air duster gun, and a needle bar. Since the sieving was conducted in a dry condition, the possibility of the loss in fines during the sieving cannot be denied. However, as Silica sand No. 8, which is used as the erodible fines particles in this experiment, is classified as fine sand, the amount of loss is minimal. The samples are taken 24 h after the end of the seepage tests. At this time, the model ground is under partially saturated conditions and the shape of the model is maintained by suction. To avoid the collapse of the model, the steel box is tilted at 301 to the upright during the sample collection. In the sampling, a thin plate is penetrated perpendicular to the side face of the model. The work is conducted with great care as quickly as possible to prevent the drying of the soil (minimum time 5 h, maximum time 8 h). The number of sampling areas for the sieve analyses is given in Table 2. Since no previous studies have reported the detailed distribution of the fines fractions in the physical model, this is one of the features of the present study.

3. Results and Discussion

3.1 *First permeation-induced change in spatial distribution of fines (Case St1)*

Fig. 5 shows the evolutions of the cumulative eroded soil mass and the variation in pore water pressure with time for *Case St1*. The left vertical axis is for the evolutions of the cumulative eroded soil mass, while the right one is for the variation in pore water pressure. The variations in pore water pressure are not directly linked to the water level. They depend on not only the hydrostatic pressure, but also the influence of the immediate fines distribution. From this figure, it can be seen that the pore water pressure increases with the increase in the water level at all the measurement points until around 0.2 h. After that, they show a peak value around an elapsed time of 0.2 h. Finally, they reach a nearly steady seepage condition.

The initiation of fines erosion is observed almost as soon as the pore water pressure, located at the bottom of the toe (P4 in Fig. 3), starts rising. Major fines erosion takes place over a period of around 0.15 h (540 s) after the detection of the eroded soil from the model. After that, the increment in eroded soil mass with time becomes small. These facts suggest that a relatively large amount of soil is eroded under the unsteady seepage condition, i.e., during the first permeation of water to the embankment.

The distribution of changes in the fines contents, normalized by the initial value, is plotted in Fig. 6 for *Case St1*. The changes in the spatial distribution of the fines are calculated by assuming that the initial fines content is the same in all parts of the model embankment before the seepage tests. In the figure, the observed phreatic surface before the end of the seepage tests is indicated by a solid line.

A decrease in fines is observed throughout the model, especially at the bottom of the foundation near the downstream boundary (Fig. 6). The majority of these changes in the spatial distribution of the fines may occur before reaching the nearly steady state. A lot of fines wash out during the first permeation and this may be attributed to the disappearance of suction due to the saturation and the reposition of fines by hydraulic force. The first arrival of seepage water may cause changes in the effective stress, resulting in small changes in the structure of the soil. A particle held in a stable position before wetting suffers hydraulic force, such as seepage force and buoyancy force, when the seepage water reaches the particle. Then, a movable particle initiates the migration or transportation. The initiation might depend on the particle size and/or the initial position in the void of the coarse skeleton. This particle migration or transportation leads to changes in the immediate local flow conditions and an infinitesimal collapse of the initial structure of the soil. As a result, fines reposition takes place. Fell et al. (2003) explained that the vulnerability to dam failure is greater on the first water filling or at the historic high reservoir water level. In other words, marked changes in hydraulic stability against seepage of an embankment occur during the wetting.

3.2 *Characteristics of erosion under the steady seepage flow*

Fig. 7 shows the evolutions of the cumulative eroded soil mass for *Cases St20*, *St24*, and *St48* and the discharge rate of water at the toe, with the exception of *Case St1*. The right vertical axis is for the normalized mass of erosion. The eroded soil ratio in Table 2 and the normalized mass of erosion in Figs. 7 and 12 are calculated by normalizing the cumulative eroded soil mass by the total fines (Silica sand No. 8) in the model before the seepage tests. In *Case St48*, the data are not collected continuously. The ending total eroded soil masses are as summarized in Table 2. As shown in Fig. 7, major fines erosion takes place in the early stage of the seepage tests (until around 1–4 h). In this period, the discharge rate is relatively large. After that, the erosion rates get smaller and the discharge rate also gradually decreases with time to 0.4–0.6 L/min.

Some discrepancy in the cumulative eroded soil mass exists, i.e., the eroded soil mass is relatively large in *Case St280* (see Table 2) and the discharged rate is also large in this case, compared with the other cases. The exact causes are unclear, but the authors infer the occurrence of a relatively strong flow between the sidewall and the soil in this case. However, as the spatial distributions of fines fractions in the middle cross section in this case show a coherent trend, compared with the other cases, this test result is also used to discuss the progress of suffusion in the following subsections.

The main cause of the fines erosion in the early stage of the seepage tests is attributed to the disappearance of suction due to water permeation and the reposition of fines by hydraulic force, as described above. After a certain elapsed time, the evolution of suffusion slowly continues under the nearly steady seepage conditions in the embankment, as described by Luo et al. (2012), for the one-dimensional seepage tests, i.e., fine particles migration-pores clogging-pushing out clogging pores-fine particles remigration.

The distributions of the changes in the percentage of the fines contents normalized by the initial value are plotted in Fig. 8 for all the cases. After a certain elapsed time, it became difficult to observe the accurate phreatic surface for the wetting of the soil. Thus, the phreatic surface could not be observed except in the case of *Case St1*. Therefore, in the figure, the observed phreatic surface before the end of *Case St1* is indicated by a solid line to show the approximate position of the phreatic surface for each case. All the results show that the fines content decreases as a whole, especially for elements near the downstream boundary. A decrease in fines in the elements near the upstream boundary is also seen because of the absence of a supply of fines from the upstream. The following can be observed from the figure:

- In *Cases St24*, *St48*, and *St280* (Fig. 8(b)–(d)), a regressive decrease in fines along the phreatic surface is observed from the middle of the foundation near the downstream boundary.
- In *Case St20*, an increase in the fines content is observed in some elements.
- In *Case St48*, although the seepage time for *Case St48* is longer than that for *Cases St20* and *St24*, the cumulative eroded soil mass for *Case St48* is relatively small.
- In *Case St280*, the magnitude of change in the spatial distribution of fines is large compared with that in the other cases. It also shows an increase in fines in the foundation, horizontally 30 mm and 280 mm in distance from the toe of the slope.

As shown in Fig. 7, the erosion rate correlates to the flow rate. In other words, the transportation of particles correlates with the hydraulic conductivity of the entire embankment. During the steady seepage, the erosion rates get smaller and the discharge rate also gradually decreases with time. Previous one-directional seepage tests showed a similar trend, i.e., a decrease in hydraulic conductivity with elapsed time (e.g., Lafleur, 1999; Bendahmane et al., 2008; Marot et al., 2012), as can be observed in Fig. 7. The decrease in hydraulic conductivity may be the result of the suffusion-induced clogging in the soil specimen. Lafleur (1999) showed that the variations in general hydraulic conductivity of a specimen depend on the spatial distribution of fines in the specimens in their interpretation of downward filtration tests on geotextiles and cohesionless soils. If this interpretation is applied to the present study, it can be said that the permeability of the whole embankment depends on the spatial distribution of the fines fraction in the embankment.

To understand the progress of suffusion in the embankment under a steady seepage flow, an attempt is made to visualize the changes in the fines content distribution using the tests with different seepage times. Assuming all initial test conditions and erosion processes are the same, the tests are arranged in ascending order of the seepage time or cumulative eroded mass. To eliminate the changes in fines content during the transient stage, i.e., before the seepage flow becomes stable, the distributions of the changes in the incremental percentage in the fines content, making Case St1 a reference, are plotted in Fig. 9.

It is not very clear, but a decrease in fines is observed in the slope zone and in the upper half of the foundation, while an increase in fines can be seen in the bottom half of the foundation over one or two days of steady seepage (Fig. 9 (a)–(c)). This contrast becomes clearer with the elapse time. In *Case St280*, many fines are eroded out (it should be noted, however, that the discharge rate in this case is larger than in the other cases) and a large decrease in fines occurred in Area B near the toe and in Area C near the phreatic surface in the slope zone (Fig. 9(d)).

An increase in fines can be observed at the bottom of the foundation around horizontally 0–70 mm and 315–385 mm in distance from the toe of the slope under a steady seepage flow. These areas of increased fines develop in the horizontal direction with time. As the seepage flow is mostly horizontal at the foundation, leftward horizontal migration of the fines is expected. However, the decreasing rate at element A is relatively small, compared with the increasing rate at the further downstream locations at the bottom of the foundation. A possible explanation for this is the migration of fines in the other directions. In other words, the eroded fines move not only by the seepage flow, but also by the gravitational vertical force, and deposit in the foundation. This local concentration of fines in the embankment may cause a decrease in the permeability of the whole embankment, as shown in Fig. 7, which is consistent with the interpretation of the elemental tests by Lafleur (1999).

3.3 *Effect of repeated permeation*

To investigate the characteristics of erosion in a regular pattern of the rising and falling phreatic surface, focus is placed on the results of *Case St96RS4*, which show a well-controlled boundary water level and regular repeated permeations. Fig. 10 shows evolutions of the cumulative eroded soil mass at each of the seepage periods for *Case St96RS4*. This result shows that the erosion of fines occurs mostly during the first seepage period. From the second period, the eroded mass decreases. In all seepage periods, major fines erosion takes place in the early stage (until around 5 h). The measured cumulative eroded soil mass at the beginning of each seepage period shows a negative value, as presented in Fig. 10. The exact causes are unclear, but the authors infer that the fluctuation in the water surface in the plastic container shown in Fig. 3(b) is due to some trouble leading to a variation in measurement values.

Changes in the discharge rate of the water at the toe, for each seepage period in *Case St96RS4*, are shown in Fig. 11. In this figure, it is observed that the discharge rate of water increases slightly from the third seepage period. This means that the permeability of the whole embankment increases with the increasing times of repeated permeation.

Fig. 12 shows the evolutions of the cumulative eroded soil mass for *Cases St280* and *St280RS40*. In *Case St280RS40*, the discharge rate of water is not measured. However, according to the evolutions of the cumulative eroded soil mass at the first seepage period for *Cases St280* and *St280RS40*, the discharge rate of water for *Case St280RS40* is expected to be the same level.

The distribution of the changes in the percentage of the fines contents is plotted in Fig. 13 for *Cases St96RS4*, *St96RS8*, and *St280RS40*. The following trend in the changes in the spatial distribution of fines can be understood from each figure:

- In *Case St96RS4*, a decrease in fines can be seen from the middle of the foundation near the downstream boundary (Fig. 13(a)).
- In *Case St96RS8*, a decrease in fines can be confirmed from the middle of the foundation near the downstream boundary and the upper part of the slope zone (Fig. 13(b)). A high concentration of fines is observed around the middle of the slope zone below the phreatic surface.
- In *Case St280RS40*, a decrease in fines can be observed from the middle of the foundation near the downstream boundary to the lower section of the crown. The increase in fines at the foundation zone is larger and more extensive than for the other cases (Fig. 13(c)).

The major fines erosion in the early stage of each seepage period, shown in Fig. 10, is attributed to the disappearance of suction due to the saturation and the reposition of fines by hydraulic force, as described in the previous subsections.

To understand the effect of the repeated permeations on the spatial distribution of fines, the results of sieve analyses for *Cases St280* and *St280RS40* are compared. The distribution of the changes in the incremental percentage of the fines content, making *Case St280* a reference, is plotted in Fig. 14 for *Case St280RS40*. From the figure, the clear boundary D–D' that separates the areas of increase and decrease of fines is seen. This indicates that a number of fines are transported from decreased elements to elements located just below or obliquely downward due to repeated permeations. In other words, repeated permeations lead to the prominent vertical transportation of fines around the boundary between the slope zone and the foundation zone. The causes of this formation of the clear boundary at D–D' remain unknown, but it can be said that the drawdown between cycles allows the transported fines to settle and this is one of the reasons for the marked increase in fines in the foundation zone.

4. Conclusions

In this paper, a series of physical model tests on seepage- induced suffusion in a homogeneous embankment has been conducted. Binary mixtures, consisting of two Silica sands (Silica sands Nos. 3 and 8) with different dominant particle sizes, have been used for the model embankment. The seepage-induced temporal and spatial variations in the fines contents in the embankment have been examined through sieve analyses on subdivided areas of the model embankment after seepage testing, and the following conclusions are drawn:

1. Seepage-induced suffusion in an embankment can be reproduced with a small-scale loosely compacted levee model in the laboratory.
2. Sieve analyses in each area of the embankment can help to successfully observe the spatial distribution of fines within the model embankment.
3. Under the transient seepage condition in the first permeation, major fines erosion takes place due to the rising phreatic surface. The disappearance of suction and the transportation of fines with the seepage flow change the distribution of the fines content in the embankment.
4. After a certain elapsed time, suffusion backwardly develops along the phreatic surface from downstream in the embankment. Below the phreatic surface, the erodible fines not only move laterally by the seepage flow, but also vertically due to the gravitational force, and are deposited in the foundation. This deposition of the fines results in the expansion of the fine-rich region in the foundation and causes a decrease in the permeability of the whole embankment. In addition, it has been confirmed that repeated permeations lead to the prominent vertical transportation of fines from the slope zone to the foundation zone.

Acknowledgements

This work was supported by JSPS KAKENHI, Grant number 25420498.

References

Beguin, R., Fry, J. J., Picault, C., Courivaud, J. R., Faure, Y. H., Philippe, P., 2012. Control of the risk of dike failure caused by contact erosion. In: Proceedings of 6th International Conference on Scour and Erosion, Paris, pp. 1551–1558.

Bendahmane, F., Marot, D., Alexis, A., 2008. Experimental parametric study of suffusion and backward erosion. J. Geotech. Geoenviron. Eng. 134 (1), 57–67.

Chang, D.S., Zhang, L.M., 2013. Extended internal stability criteria for soils under seepage. Soils Found. 53 (4), 569–583.

Cividini, A., Bonomi, B., Vignati, G.C., Gioda, G., 2009. Seepage-induced erosion in granular soil and consequent settlements. Int. J. Geomech. 9 (4), 187–194.

Cividini, A., Gioda, G., 2004. Finite-element approach to the erosion and transport of fine particles in granular soils. Int. J. Geomech. 4 (3), 191–198.

Fell, R., Fry, J.J., 2013. State of the art on the likelihood of internal erosion of dams and levees by means of testing. In: Bonelli, S. (Ed.), Erosion in Geomechanics Applied to Dams and Levees. ISTE-Wiley, Londan, UK, pp. 1–99 Chapter 1.

Fell, R., Wan, C.F., Cyganiewicz, J., Foster, M., 2003. Time for development of internal erosion and piping in embankment dams. J. Geotech. Geoen- viron. Eng. 129 (4), 307–314.

Foster, M., Fell, R., 1999. A framework for estimating the probability of failure of embankment dams by internal erosion and piping using event tree methods. University of New South Wales, Sidney UNICIV reports.

Foster, M., Fell, R., 2001. Assessing embankment dam filters that do not satisfy design criteria. J. Geotech. Geoenviron. Eng. 127 (5), 398–407.

Foster, M., Fell, R., Spannagle, M., 2000. The statistics of embankment dam failures and accidents. Can. Geotech. J. 37 (5), 1000–1024.

Fry, J.J., 2012. Introduction to the process of internal erosion in hydraulic structures: embankment dams and dikes. In: Bonelli, S. (Ed.), Erosion of Geomaterials. ISTE-Wiley, London, UK, pp. 1–36 Chapter 1.

Fry, J.J., Vogel, A., Royet, P., Courivaud, J.R., 2012. Dam failures by erosion: lessons from ERINOH data bases. In: Proceedings of 6th International Conference on Scour and Erosion, Paris, pp. 273–280.

Honjo, Y., Haque, M. A., and Tsai, K. A., 1996. Self-filteration behavior of broadly and gap graded cohesionless soils. In: Proceedings of 2nd International Conference on Geofilters, Montreal, pp. 227–236.

Ke, L., Takahashi, A., 2012. Strength reduction of cohesionless soil due to internal erosion induced by one-dimensional upward seepage flow. Soils Found. 52 (4), 698–711.

Ke, L., Takahashi, A., 2014. Experimental investigations on suffusion characteristics and its mechanical consequences on saturated cohesionless soil. Soils Found. 54 (4), 713–730.

Kenney, T.C., Lau, D., 1985. Internal stability of granular filters. Can. Geotech. J. 22 (2), 215–225.

Khomenko, V.P., 2006. Suffosion hazard: Today's and tomorrow's problem for cities. In: Proceedings of the 10th IAEG International Congress, Notting- ham, pp. 1–8.

Kuwano, R., Kohata, Y., Sato, M., 2012. A case study of ground cave-in due to large scale subsurface erosion in old land fill. In: Proceedings of 6th International Conference on Scour and Erosion, Paris, pp. 265–271.

Ladd, R.S., 1978. Preparing test specimens using undercompaction. Geotech. Test. J. 1 (1), 16–23.

Lafleur, J., 1999. Selection of geotextiles to filter broadly graded cohesionless soils. Geotext. Geomembr. 17 (5–6), 299–312.

Li, M., Fannin, R.J., 2008. Comparison of two criteria for internal stability of granular soil. Can. Geotech. J. 45 (9), 1303–1309.

Lindow, N., Fox, G., Evans, R., 2009. Seepage erosion in layered stream bank material. Earth Surf. Process. Landf. 34, 1693–1701.

Luo, Y., Qiao, L., Liu, X., Zhan, M., Sheng, J., 2012. Hydro-mechanical experiments on suffusion under long-term large hydraulic heads. Nat. Hazards 65 (3), 1361–1377.

Marot, D., Bendahmane, F., Nguyen, H.H., 2012. Influence of angularity of coarse fraction grains on internal erosion process. In: Proceedings of 6th International Conference on Scour and Erosion, Paris, pp. 887–894.

Moffat, R., Fannin, R.J., 2011. A hydromechanical relation governing internal stability of

cohesionless soil. Can. Geotech. J. 48 (3), 413–424.
Moffat, R., Fannin, R.J., Garner, S.J., 2011. Spatial and temporal progression of internal erosion in cohesionless soil. Can. Geotech. J. 48 (3), 399–412.
Moraci, N., Mandaglio, M.C., Ielo, D., 2014. Analysis of the internal stability of granular soils using different methods. Can. Geotech. J. 51 (9), 1063–1072.
Perzlmaier, S., Muckenthaler, P., Koelewijn, A.R., 2007. Hydraulic criteria for internal erosion in cohesionless soil. In: Fell, R., Fry, J.J. (Eds.), Internal Erosion of Dams and Their Foundations. Taylor & Francis Group, London, UK, pp. 179–190.
Richards, K.S., Reddy, K.R., 2007. Critical appraisal of piping phenomena in earth dams. Bull. Eng. Geol. Environ. 66 (4), 381–402.
Richards, K.S., Reddy, K.R., 2012. Experimental investigation of initiation of backward erosion piping in soils. Géotechnique 62 (10), 933–942.
Richards, K.S., Reddy, K.R., 2014. Kinetic Energy Method for predicting initiation of backward erosion in earthen dams and levees. Environ. Eng. Geosci. 20 (1), 85–97.
Saito, Y., Kuwano, R., Sasaki, T., 2012. The model tests on a permeability of ground against repeated process of seepage. In: Proceedings of the 47th Japan National Conference on Geotechnical Engineering, Hachinohe, pp. 903–904. (In Japanese).
Skempton, A.W., Brogan, J.M., 1994. Experiments on piping in sandy gravels. Géotechnique 44 (3), 449–460.
Sterpi, D., 2003. Effects of the erosion and transport of fine particles due to seepage flow. Int. J. Geomech. 3 (1), 111–122.
Terzaghi, K., 1939. Soil mechanics: a new chapter in engineering science. J. Inst. Civil Eng. 12 (7), 106–142.
Tomlinson, S.S., Vaid, Y.P., 2000. Seepage forces and confining pressure effects on piping erosion. Can. Geotech. J. 37 (1), 1–13.
Uzuoka, R., Ichiyama, T., Mori, T., Kazama, M., 2012. Hydro-mechanical analysis of internal erosion with mass exchange between solid and water. In: Proceedings of 6th International Conference on Scour and Erosion, Paris, pp. 655–662.
Wan, C., Fell, R., 2008. Assessing the potential of internal instability and suffusion in embankment dams and their foundations. J. Geotech. Geoenviron. Eng. 134 (3), 401–407.
Zhang, X., Dong, J., Huang, Z., Nie, X., Wong, H., Wang, J.X., 2014. Study of soil structures strength and stiffness loss based on thermodynamics and continuum mechanics. Environ. Earth Sci..
Zhang, X.S., Wong, H., Leo, C.J., Bui, T.A., Wang, J.X., Sun, W.H., Huang, Z.Q., 2013. A thermodynamics-based model on the internal erosion of earth structures. Geotech. Geol. Eng. 31 (2), 479–492.

Table 1 Physical properties of tested soils

Physical property	Silica sand No. 3 (Coarse fraction)	Silica sand No. 8 (Fines)	Mixture
Specific gravity, G_s	2.645	2.645	2.645
Fines content, FC (%)	——	——	15
Maximum void ratio, $e_{\max}$	0.94	1.33	0.79
Minimum void ratio, $e_{\min}$	0.65	0.7	0.53
Median particle size D_{50} (mm)	1.76	0.16	1.78
Effective particle size D_{10} (mm)	1.37	0.087	0.138
Uniformity coefficient, C_u	1.5	1.7	13
Curvature coefficient, C_c	1.1	0.96	7.9
Grain Description	Sub-rounded ~ Sub-angular		

Table 2 Test cases of seepage testing

Case	Dry density (Mg/m^3)	Seepage time (hr)	Repeat count of supply and drainage	Number of sampling areas	Cumulative eroded soil mass (g)	Eroded soil ratio (%)
St1	1.559	0.55	1	48	22.77	0.764
St20	1.562	20	1	48	32.37	1.085
St24	1.560	24	1	48×3	34.88	1.169
St48	1.567	48	1	66	28.03	0.913
St280	1.560	280	1	45	154.67	5.190
St96RS4	1.560	96	4	48	44.55	1.495
St96RS8	1.560	96	8	95	43.11	1.447
St280RS40	1.559	280	40	47	234.82	7.885

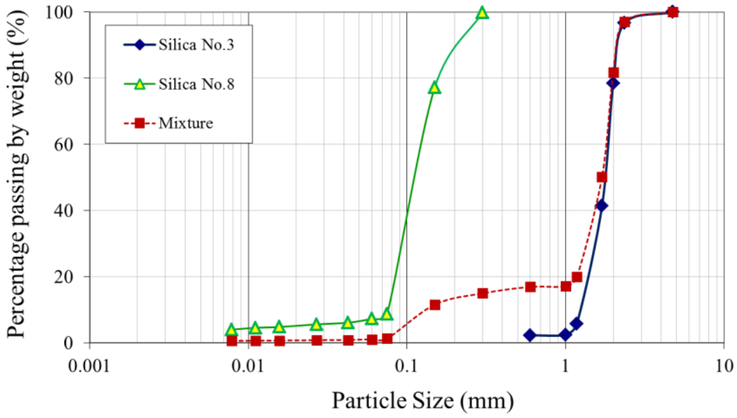

Fig.1. Grain size distribution curves of silica sands and their mixture

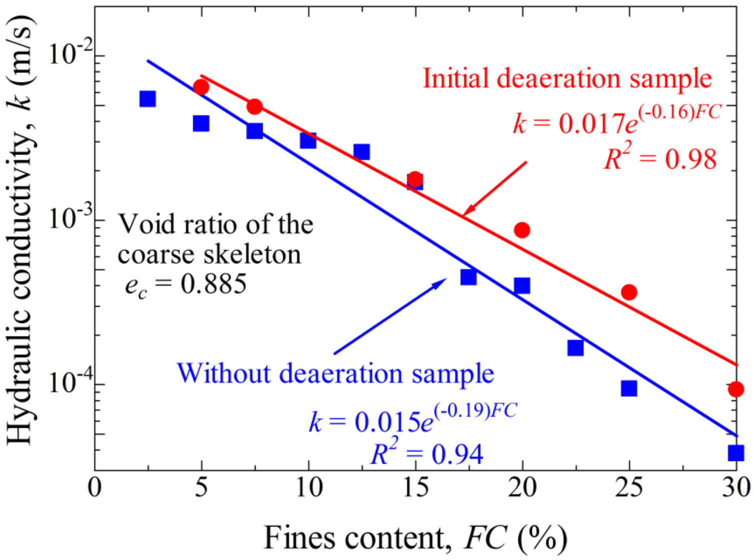

Fig.2. Relationships between fines content and permeability under constant void ratio of coarse skeleton

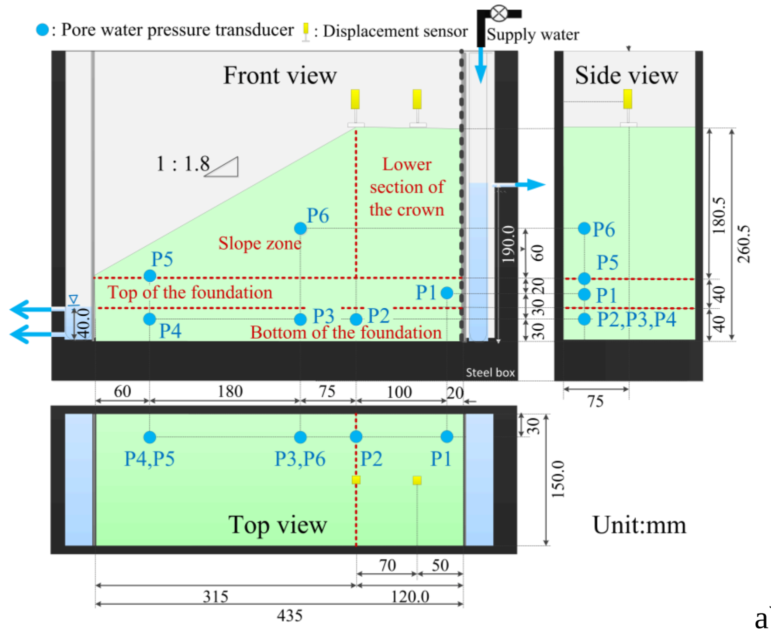

a)

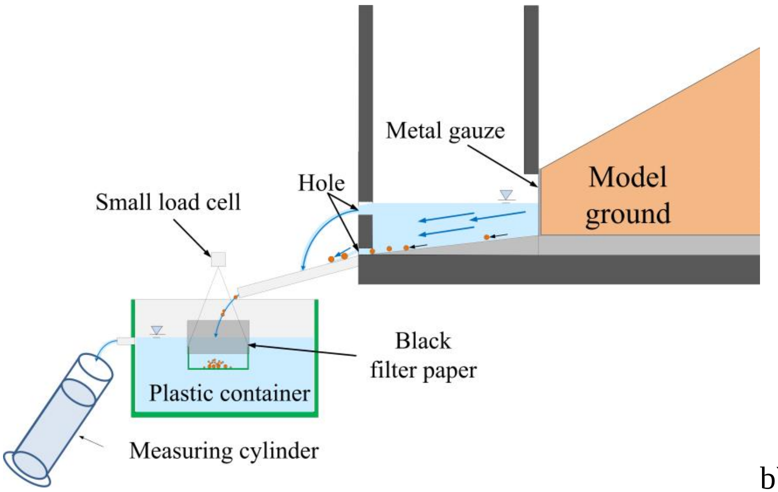

b)

Fig. 3. Schematic diagram of experimental system, (a) physical model, (b) Sampling on eroded fines

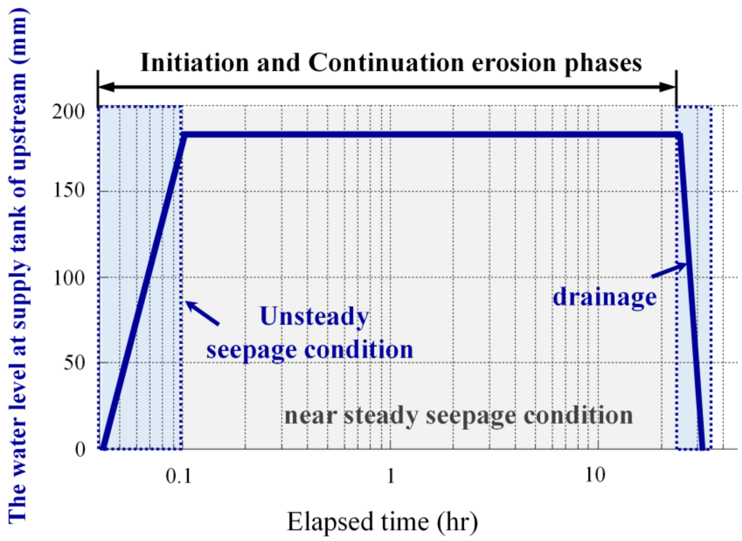

Fig. 4. Conceptual diagram of controlled water level at water supply tank

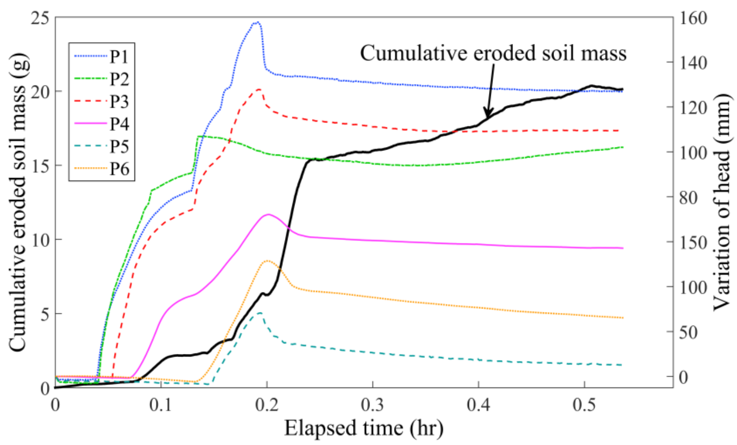

Fig. 5. Evolutions of cumulative eroded soil mass and variation of pore water pressure for *Case St1*

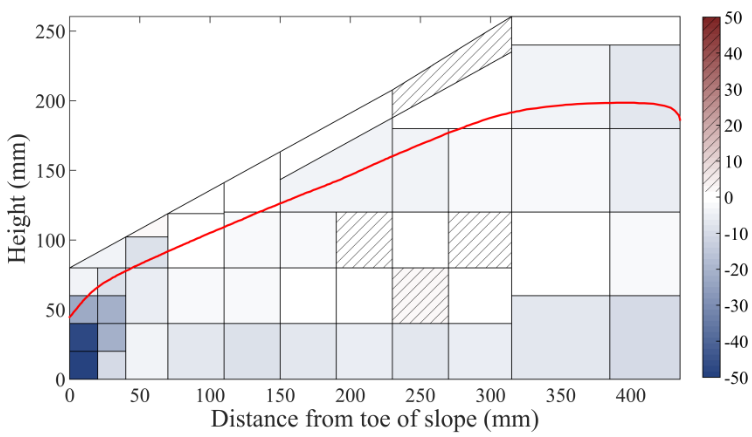

Fig. 6. Distribution of percentage change in fines content for *Case St1*

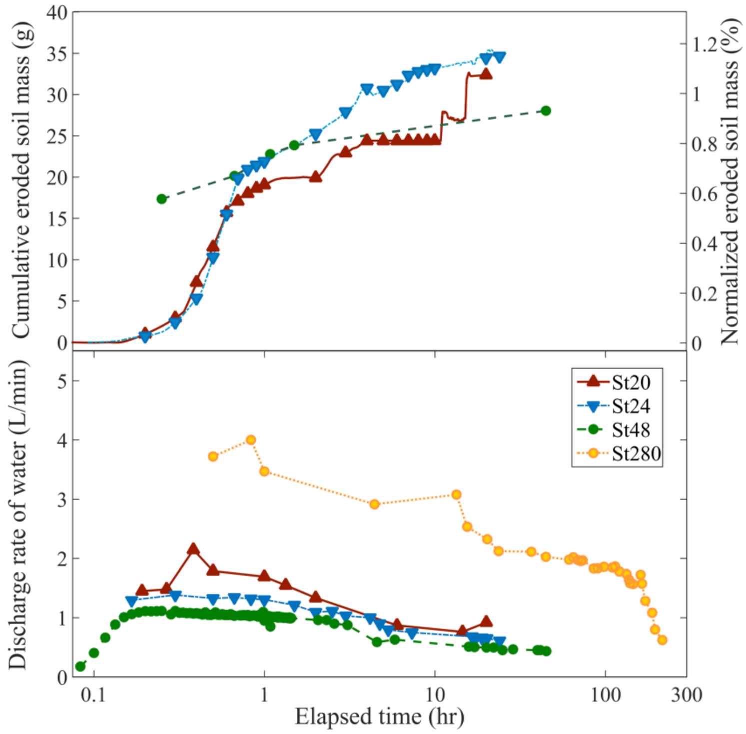

Fig. 7. Evolutions of cumulative eroded soil mass for *Cases St20*, *St24* and *St48* and evolutions of discharge rate of water for *Cases St20*, *St24*, *St48* and *St280*

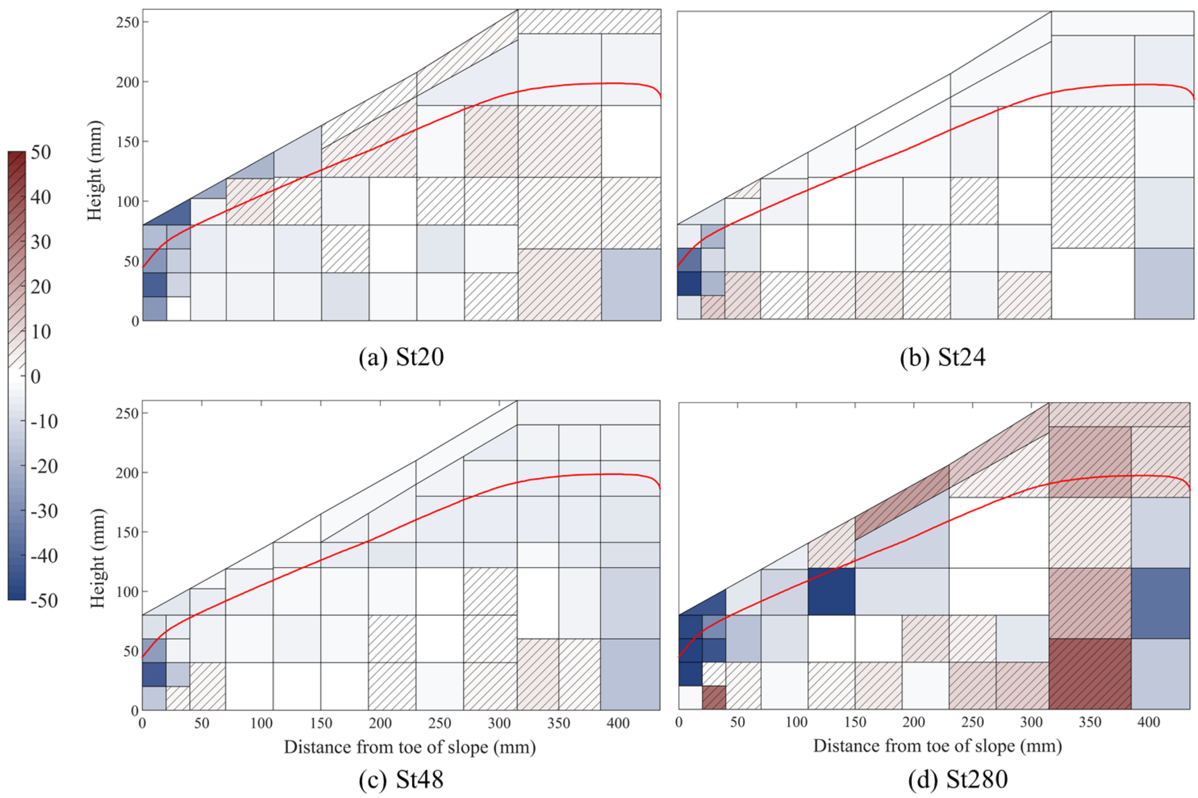

Fig. 8. Distributions of percentage change in fines content for *Cases St20*, *St24*, *St48* and *St280*

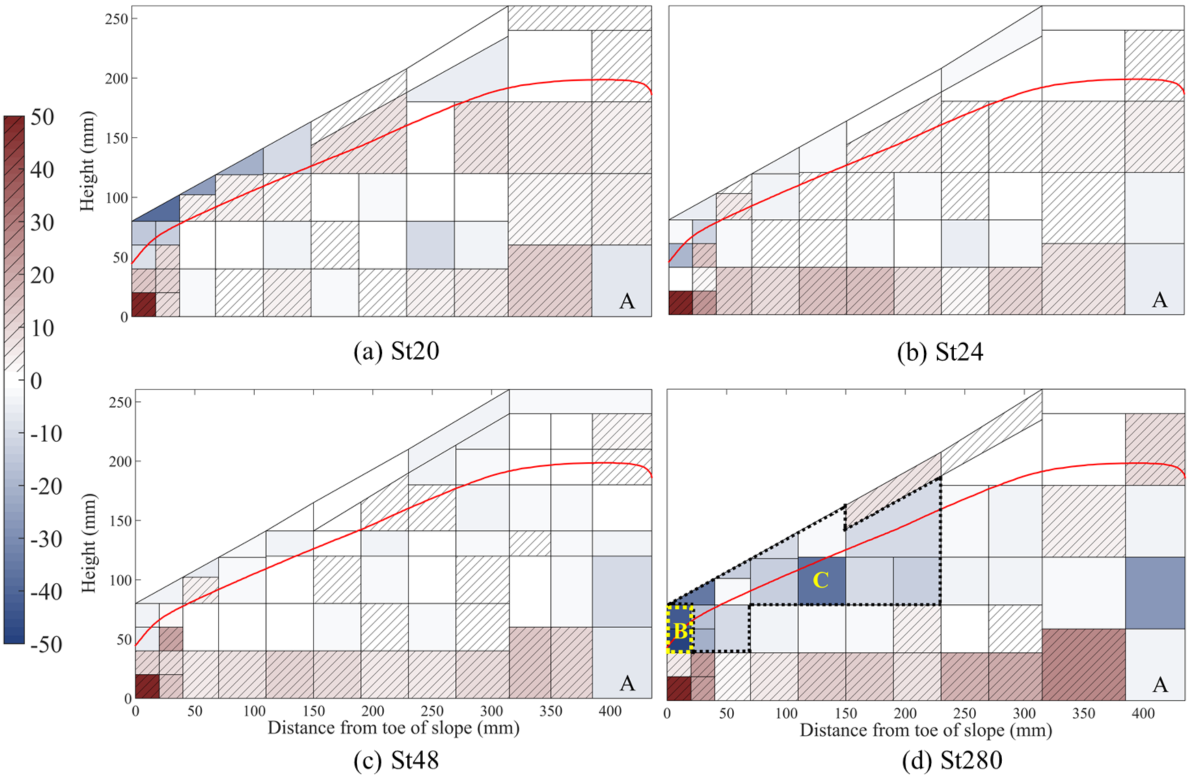

Fig. 9. Distributions of incremental percentage change in fines content by making Case St1 as a reference, (a) *Case St20* (20 hours), (b) *Case St24* (24 hours), (c) *Case St48* (48 hours), (d) *Case St 280* (280 hours)

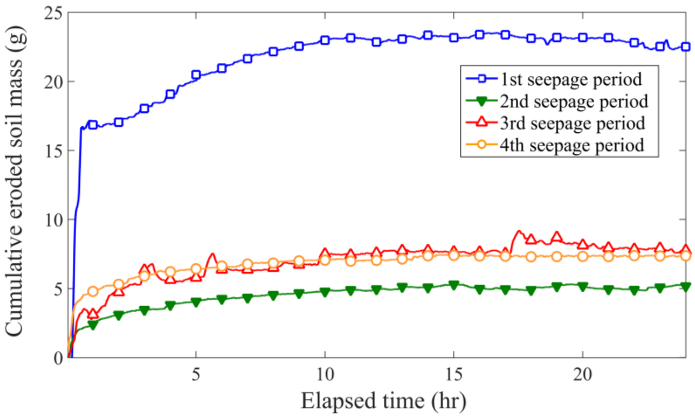

Fig. 10. Evolutions of cumulative eroded soil mass at each seepage period for *Case St96RS4*

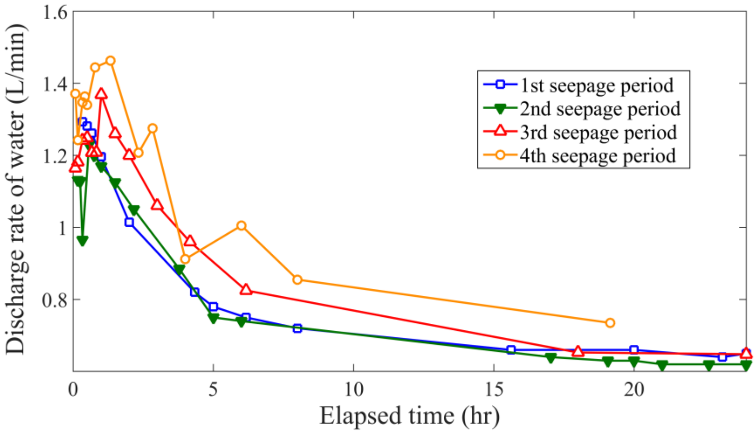

Fig. 11. Evolutions of discharge rate of water for *Case St96RS4*

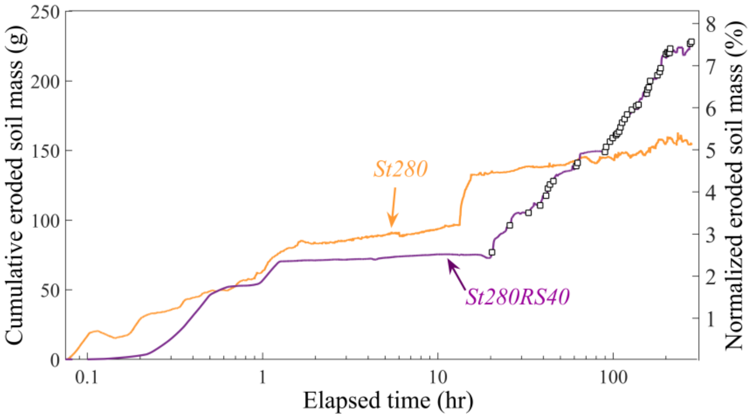

Fig. 12. Evolutions of cumulative eroded soil mass for *Cases St280* and *St280RS40*

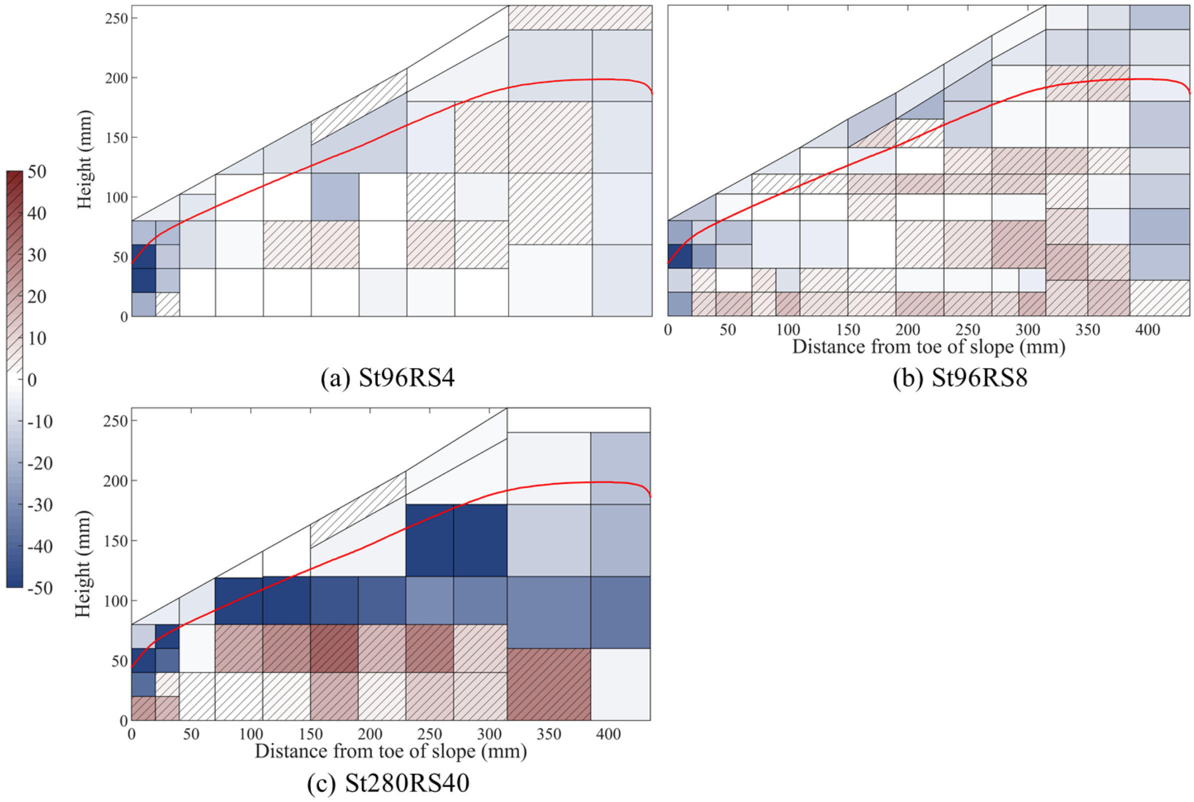

Fig. 13. Distributions of percentage change in fines content for *Cases St96RS4*, *St96RS8* and *St280RS40*

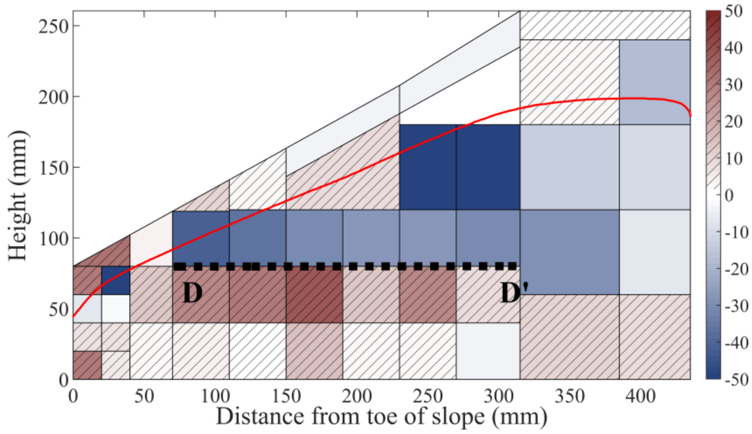

Fig. 14. Distribution of incremental percentage change in fines content by making *Case St280* as a reference for *Case St280RS40*